END

FILMED

DTIC

MICROCOPY RESOLUTION TEST CHART

NATIONAL BUREAU OF STANDARDS-1963-A

OFFICE OF NAVAL RESEARCH

TECHNICAL REPORT NO. 44

Surface Enhancement Factors For Raman Scattering

At Silver Electrodes. Role of Adsorbate-Surface

Interactions and Electronic Structure.

by

Michael J. Weaver, Stuart Farquharson, M. A. Tadayyoni

Prepared for Publication

in the

Journal of Chemical Physics

Department of Chemistry

Purdue University

West Lafayette, IN 47907

August 1985

85 10 7 105

REPORT DOCUMENTATION PAGE

READ INSTRUCTIONS
BEFORE COMPLETING FORM

1. REPORT NUMBER	2. GOVT ACCESSION NO.	3. RECIPIENT'S CATALOG NUMBER
Technical Report No. 44		

4. TITLE (and Subtitle)

Surface Enhancement Factors For Raman Scattering At Silver Electrodes. Role of Adsorbate-Surface Interactions and Electronic Structure.

5. TYPE OF REPORT & PERIOD COVERED

Technical Report No. 44

6. PERFORMING ORG. REPORT NUMBER

7. AUTHOR(s)

Michael J. Weaver, Stuart Farquharson, and M. A. Tadayyoni

8. CONTRACT OR GRANT NUMBER(s)

N00014-79-C-0670

9. PERFORMING ORGANIZATION NAME AND ADDRESS

Department of Chemistry
Purdue University
West Lafayette, IN 47907

10. PROGRAM ELEMENT, PROJECT, TASK AREA & WORK UNIT NUMBERS

11. CONTROLLING OFFICE NAME AND ADDRESS

Office of Naval Research
Department of the Navy
Arlington, VA 22217

12. REPORT DATE

August 1985

13. NUMBER OF PAGES

14. MONITORING AGENCY NAME & ADDRESS(If different from Controlling Office)

15. SECURITY CLASS. (of this report)

Unclassified

15a. DECLASSIFICATION/DOWNGRADING SCHEDULE

16. DISTRIBUTION STATEMENT (of this Report)

Approved for Public Release; distribution unlimited

Accession For

NTIS CRA&I ☒
DTIC TAB ☐
Unannounced ☐
Justification

17. DISTRIBUTION STATEMENT (of the abstract entered in Block 20, If different from Report)

Block #5 above changed
By _per telecon. JC_
Distribution /

Availability Codes

18. SUPPLEMENTARY NOTES

Dist | Avail and/or Special

A-1

19. KEY WORDS (Continue on reverse side if necessary and identify by block number)

Raman scattering cross sections, electronic resonance, excitation profile

20. ABSTRACT (Continue on reverse side if necessary and identify by block number)

The integrated Raman band intensities for internal vibrational modes of various adsorbates at roughened silver electrodes are combined with surface concentrations obtained electrochemically to yield surface Raman scattering cross sections. These data together with the corresponding bulk-phase Raman intensities provide stimates of the degree of enhancement of the vibrational bands at the silver surface with respect to the bulk medium, i.e., the "surface enhancement factors", SEF. For surface-attached thiocyanate, isothiocyanate-bridged Cr(III) complexes, and also for Cr(III) and Co(III) hexaammines that

DD FORM 1 JAN 73 **1473**

SURFACE ENHANCEMENT FACTORS FOR RAMAN SCATTERING

AT SILVER ELECTRODES. ROLE OF ADSORBATE-SURFACE

INTERACTIONS AND ELECTRONIC STRUCTURE.

Michael J. Weaver*, Stuart Farquharson, and M. A. Tadayyoni

Department of Chemistry, Purdue University
West Lafayette, IN 47907

Abstract

The integrated Raman band intensities for internal vibrational modes
of various adsorbates at roughened silver electrodes are combined with
surface concentrations obtained electrochemically to yield surface Raman
scattering cross sections. These data together with the corresponding
bulk-phase Raman intensities provide estimates of the degree of enhancement
of the vibrational bands at the silver surface with respect to the bulk
medium, i.e., the "surface enhancement factors" (SEF). For surface-attached
thiocyanate, isothiocyanate-bridged Cr(III) complexes, and also for
Cr(III) and Co(III) hexaammines that are electrostatically attracted to
chloride-coated silver, SEF values are obtained that are relatively
insensitive to both the vibrational mode and the adsorbate, even though
substantial (up to 500 fold) variations are observed in the Raman cross
sections. This finding applies to stretching modes involving nonbridging
ammine groups as well as to bridging thiocyanate modes, although the
frequencies of the latter, but not of the former, are perturbed strongly
by the silver surface. Comparisons were also made between Raman cross
sections, surface enhancement factors, and excitation profiles for
pyrazinepentaammineosmium(III) and (II) to explore the influence of
electronic resonance since the Os(II) form displays an intense charge-
transfer band in the vicinity of the laser wavelengths (460-650 nm)
employed. A pronounced peak in the Os(II) excitation profile, absent
for Os(III), is obtained that is markedly (ca. 100 nm) red shifted for
the adsorbed versus bulk complex.

Introduction

Surface-enhanced Raman spectroscopy (SERS) is becoming established as a valuable surface characterization technique, especially for *in-situ* studies of adsorbates at metal-electrolyte interfaces.[1] The prosperity of SERS rests on the dramatic enhancements of the Raman scattering intensity seen for a variety of adsorbates at certain metal surfaces, most notably silver. This enables Raman spectra for the adsorbed molecules to easily be obtained even with conventional electrochemical cells containing high bulk concentrations of the Raman scatterer.

Not surprisingly, this unexpected finding has generated considerable research activity aimed at elucidating the enhancement mechanisms, and has spawned a number of theoretical treatments.[1,2] Although there is some diversity among these theories, a common viewpoint is that the observed signals arise from a combination of surface enhancement processes.[1b,d,2] Broadly speaking, these can be categorized into electromagnetic enhancement mechanisms resulting from the influence of the incident radiation on the local electric field at the surface, and surface resonance enhancement associated with electronic transitions between the adsorbate and the metal surface.

In order to properly utilize SERS as a surface chemical probe as well as to understand the role of such factors it is clearly important to obtain quantitative information on the efficiency of surface Raman scattering as a function of the adsorbate structure and the type of adsorbate-surface interactions involved. It is useful to define a "surface enhancement factor," SEF, as the ratio of the Raman scattering efficiency of a given internal vibrational mode for the adsorbate when present at the metal surface with respect to the corresponding scattering efficiency in bulk

media.[1a] Surprisingly, however, quantitative evaluations of SEF are very sparse.[1a,3,4] The original value of SEF for pyridine at mildly roughened silver electrodes, ca. 1×10^6, is widely quoted; yet a markedly smaller value, 1.5×10^4, has been reported for a closely related system.[4]

One factor responsible for the scarcity of SEF determinations is the paucity of surface coverage data for SERS-active adsorbates at silver. However, in connection with kinetic and mechanistic studies at silver and other electrodes we have developed methods for accurately evaluating surface concentrations for both electroactive[5] and nonelectroactive species.[6] These studies have in turn identified a series of structurally simple adsorbates at silver, in particular octahedral metal complexes and the constituent adsorbing ligands. Such systems have been employed for systematic examinations of the dependence of SERS upon adsorbate surface concentration and electrode potential,[7] oxidation state,[8] electronic structure,[8,9] and the nature of the adsorbate-surface interactions.[10]

We present here evaluations of the surface and bulk-phase Raman scattering cross sections along with the resulting surface enhancement factors for a representative selection of adsorbates at silver electrodes, obtained from quantitative Raman intensity measurements together with surface concentration data. The adsorbates include Co(III), Cr(III), and Os(III)/(II) ammine complexes containing isothiocyanate, pyrazine (pz), or pyridine (py) adsorbing groups as well as the corresponding free ligands in order to examine the possible effects of varying the adsorbate electronic structure and redox state upon the SEF. Of these, $Os^{III}(NH_3)_5pz$ and $Os^{II}(NH_3)_5pz$ are of particular interest since the latter, but not the former, displays a large resonance Raman enhancement in bulk solution within the irradiation wavelengths, 450-650 nm, most usefully employed for SERS at silver. Data are also presented for $Cr(NH_3)_6^{3+}$ and $Co(NH_3)_6^{3+}$ which are

electrostatically adsorbed at the outer Helmholtz plane rather than bound

directly (i.e., specifically adsorbed) to the silver surface.[10] These are

compared with corresponding metal-ammine intensity measurements for

structurally similar surface-attached complexes in order to examine the

possible influences of adsorbate-surface binding to SERS.

Experimental

Details of, and sources to, the syntheses of most complexes used in

the present work have been given in other papers from this laboratory as

follows: chromium isothiocyanates,[9] osmium and ruthenium pyrazines and

pyridines;[8b] $Cr(NH_3)_6 \cdot Cl_3$ and $Co(NH_3)_6 \cdot Cl_3$ were prepared as in ref. 11.

Solutions of $Os^{II}(NH_3)_5pz$ were prepared *in situ* from reduction of

$Oc^{III}(NH_3)_5pz$ using sodium dithionate. Liquid pyridine and benzene were

spectroscopic grade, whereas the solid compounds and supporting electrolytes

were reagent grade, being recrystallized prior to use. Water was purified

by using a "Milli Q" system (Millipore, Inc.).

The surface-enhanced Raman (SER) cell, containing a quartz window at

its base, was positioned so that the silver face was incident at an angle

of 30° to the laser beam. The collection lens for Raman scattering was

placed at 60° to the silver surface and 90° to the incident beam. The

silver electrode was of a rotating disk construction having a disk radius

of 0.2 cm, surrounded by a teflon sheath. The electrode was mechanically

polished on a wheel successively with 5, 1, and 0.3 μm alumina immediately

prior to use. It was then mildly roughened by means of oxidation-reduction

cycles (ORC) normally consisted of one to five potential steps from

-100 mV to +350 mV vs saturated calomel electrode (s.c.e.), returning after

the accumulation of 30-40 mC cm^{-2} anodic charge. For comparison, some

SERS measurements were made following an *in situ* ORC in the electrolyte containing the adsorbate (*vide infra*).

Bulk-phase Raman intensity measurements were made using three different sample configurations. The first consisted of aqueous or dimethylsulfoxide solutions in the electrochemical cell with the same arrangement as used for SERS in order to provide closely similar scattering geometries for the bulk and surface Raman measurements. Together with the relevant concentration data, this provided a simple means of obtaining the required relative Raman scattering efficiencies in surface and bulk-phase environments (see Results section). For species for which only limited quantities were available bulk Raman intensities were obtained instead by using 1 mm capillaries in order to minimise solution volume. Nujol mulls held between glass slides were also employed with some systems in order to attain sufficiently high concentrations so to yield accurately measurable Raman intensities. Whenever feasible, systems were examined using at least two of these configurations. The bulk Raman intensities obtained with each scattering geometry were calibrated with respect to those observed for benzene using the same arrangement (*vide infra*).

The Raman scattering was examined chiefly with a SPEX 1403 double monochromator equipped with a RCA C31034 photomultiplier tube and a SPEX DPC-2 photon counter, although some measurements employed an optical multichannel analyzer (OMA) arrangement consisting of a PAR OMA-II coupled to a SPEX 1877 triplet monochromator.[9] Raman excitation was provided by Spectra Physics Model 165 Krypton (647.1 or 676.4 nm) or Argon (457.9, 488.0 or 514.5 nm) ion lasers, or a Coherent Model Cr-599 dye laser filled with Rhodamine 6G. The last-named was pumped by the Ar$^+$ laser in an "all-lines" configuration, and used to produce light at 580, 590, and 600 nm. Other experimental details are given in refs. 8b and 9.

All measurements were made at 23 ± 1°C, and all potentials were measured and are quoted versus the saturated calomel electrode (s.c.e.).

Results and Data Treatment

The surface enhancement factor, SEF, can be expressed as

$$SEF = (\frac{d\sigma}{d\Omega})_{SER} / (\frac{d\sigma}{d\Omega})_{BR} \qquad (1)$$

where $(d\sigma/d\Omega)_{SER}$ and $(d\sigma/d\Omega)_{BR}$ are the Raman scattering cross sections (cm^2 steradian^{-1} molecule^{-1}) associated with a given vibrational band for the same molecule in surface and bulk-phase environments. Although only relative values of these two quantities for each Raman scatterer are therefore required for the determination of SEF values, it is useful to evaluate approximate absolute values of $(d\sigma/d\Omega)_{BR}$ for each system by means of a calibration with a Raman scatterer having a known scattering cross section. The 992 cm^{-1} band for liquid benzene was employed for this purpose. Values of $(d\sigma/d\Omega)_{BR}$ for benzene of 1.0×10^{-29} and 2.6×10^{-29} cm^2 sr^{-1} molecule^{-1} at excitation wavelengths of 647.1 nm and 514.5 nm, respectively, are inferred from the measured value,[12] 3.25×10^{-29} cm^2 sr^{-1} molecule^{-1} at 488.0 nm by assuming that the scattering cross section is proportional to the fourth power of the incident frequency.

Measurement of the integrated band intensities for each species relative to that for liquid benzene obtained using the same geometry yielded the values of $(d\sigma/d\Omega)_{BR}$ given in Table I. The experimental conditions employed for each system are given in the footnotes; generally the values of $(d\sigma/d\Omega)_{BR}$ were found to be independent of concentration and environment (aqueous, dimethylsulfoxide, Nujol) to within the experimental reproducibility, ca. ± 30%. The majority of Raman cross sections given in Table I refer to 647.1 nm excitation; those listed within parentheses were determined using 514.5 nm light. A polarization scrambler was employed

at the spectrometer entrance slit so to eliminate polarization effects on the band intensities. For molecules containing more than one functional group responsible for the relevant vibrational mode, for example v_{CN} in $Cr(NCS)_6^{3-}$ or v_{M-NH_3} in $Cr(NH_3)_6^{3+}$, the values given in Table I actually are scattering cross sections *per functional group* rather than per molecule, $n^{-1}(d\sigma/d\Omega)_{BR}$, where n is the number of functional groups per molecule. Although somewhat unconventional, this approach aids the intercomparison of $(d\sigma/d\Omega)_{BR}$ values between structurally related species having different numbers of a given functional group, (for example, v_{CN} in $Cr(NCS)_6^{3-}$ and $Cr(NH_3)_5NCS^{2+}$, where n = 6 and 1, respectively).

Evaluation of the corresponding values of $(d\sigma/d\Omega)_{SER}$ requires: (i) determination of the effective surface concentration of Raman scatterers, and (ii) assessment of the relative collection geometries of the spectrometer arrangement for the surface and bulk-phase molecules. Both these considerations place severe restrictions on the accuracy with which the surface enhancement factors can be determined. Nevertheless, factor (ii) can be held essentially constant for a given experimental arrangement.

An approximate estimate of (ii) was obtained by using the same Raman cell for both SERS and bulk-phase Raman measurements for several systems, as noted above. For the latter, the laser beam was reflected from the polished silver surface placed, as in the SERS measurements, several millimeters from the optical window at the base of the cell. The beam was defocussed so to provide an effective "cylinder" of irradiated solution about 1-2 mm diameter between the optical window and the silver surface. The estimate of the cylinder volume, V_{BR}, within which bulk Raman scattering occurred also took into account the path length of the light beam that is reflected back from the silver surface. For the SERS measurements, the laser beam formed an image of ca. 2 mm diameter at the electrode surface, which defined an

area, A_{SER}, within which surface Raman scattering occurred. By assuming

that the collection efficiency of the Raman scattered light was the same

in the bulk and surface Raman configurations, the desired surface Raman

scattering cross section can be found from

$$\left(\frac{d\sigma}{d\Omega}\right)_{SER} = \frac{N_{BR}I_{SER}}{N_{SER}I_{BR}} \left(\frac{I_{BR}^{i}}{I_{SER}^{i}}\right) \left(\frac{d\sigma}{d\Omega}\right)_{BR}$$

$$= \frac{V_{BR}C_{b}I_{SER}}{A_{SER}\Gamma I_{BR}} \left(\frac{I_{BR}^{i}}{I_{SER}^{i}}\right) \left(\frac{d\sigma}{d\Omega}\right)_{BR} \tag{2}$$

In Eq. (2), N_{BR} and N_{SER} are the numbers of Raman scatters, I_{BR} and I_{SER}

are the integrated Raman intensities; and I_{BR}^{i} and I_{SER}^{i} are the intensities

of the incident radiation in the bulk and surface Raman measurements,

respectively; and C_{b} and Γ are the concentrations of the Raman scatterer

in the bulk and surface environments, respectively. Commonly $I_{BR} \sim I_{SER}$;

the laser intensities were typically ca. 50-100 mW at the sample. All the

SER bands were found to be essentially depolarized (i.e., $\rho \cong 0.7$-0.75).

The surface concentrations, Γ, were evaluated using one of two methods.

The first involved measurements of the differential electrode capacitance,

C_{dl}, against the electrode potential, E, for a family of bulk adsorbate

concentrations, the C_{dl}-E curves being doubly integrated using the

"Hurwitz-Parsons" analysis.[6a] This is applicable to adsorbates that are

electroinactive over a wide potential range. Details of these measurements

for NCS⁻ at silver are available elsewhere.[6a,7a] Values of Γ for pyridine

and pyrazine were obtained using a similar procedure, double integrating

the C_{dl}-E curves from a sufficiently negative potential (beyond ca. -1.4v)

where adsorption is likely to be small on the basis of the invariance of

C_{dl} to addition of pyridine or pyrazine under these conditions.[13]

Surface concentrations for the various electroactive metal complexes were evaluated by employing rapid linear sweep voltammetry, using sufficiently low bulk concentrations (ca. 50 $\mu\underline{M}$) and high sweep rates (> 10v. sec^{-1}) so that the voltammetric peak is assocated almost entirely with the initially adsorbed, rather than diffusing, reactant.[5a] Details of these measurements for the thiocyanate complexes are given in ref. 5a, for hexaamminecobalt(III) in ref. 14, and for the osmium pyridine and pyrazine complexes in ref. 8b. Although $Cr(NH_3)_6^{3+}$ is not reduced within the potential range available at silver prior to hydrogen evolution, it is reasonable to take the adsorption to be similar to that for $Co(NH_3)_6^{3+}$. Both these species are adsorbed at silver in 0.1 $\underline{M}$ KCl via electrostatic attraction to the surface-bound chloride monolayer.[6a,14] The surface concentrations for each adsorbate given in Table I refer to the conditions (bulk adsorbate concentration, electrode potential) at which the listed values of $(d\sigma/d\Omega)_{SER}$ were obtained from Eq. (2). (See Table I and footnotes for details.[16]) These conditions were chosen so to expedite the measurement of Γ and to stabilize the appropriate oxidation state in the case of the electroactive transition-metal adsorbates. The Γ values for most systems approach those expected for a close-packed monolayer given the roughness factor (ca. 1.5 to 2.5[16]) of the silver surface. The tenacious adsorption displayed by most systems largely precluded measurements of the dependence of I_{SER} upon Γ. However, a proportionality between I_{SER} and Γ was established for $Co(NH_3)_6^{3+}$ with Γ values between 1.5 and 5 $\times$ 10^{-11} mole cm^{-2}.

The resulting values of $(d\sigma/d\Omega)_{SER}$, and the SEF values obtained from this quantity and $(d\sigma/d\Omega)_{BR}$ using Eq. (1), are also listed in Table I. These data were obtained by electrochemically roughening the electrode in a separate 0.1 $\underline{M}$ KCl solution followed by rapid transferral to the Raman cell (*vide supra*). Although the resulting SERS signals became more intense

as the numbers of ORC's was increased up to five, the SEF values are relatively unaffected (within the experimental reproducibility; ca. 1.5 fold) since the electrode roughness factor also increases under these conditions.[6a,16] Raman intensity measurements were made as rapidly as possible (usually ≤ 5-10 mins; < 1 min when using the OMA) so to minimize the temporal decay of the SERS signals.[7a] Oxidation-reduction cycles performed in the cell solutions of interest containing chloride usually yielded ca. 1.5-3 fold higher SEF values. This procedure, however, suffers from the risk of trapping undetermined amounts of adsorbate in the deposited silver layer. Again, the surface Raman cross-section and SEF values listed without and within parentheses in Table I were determined using 647.1 and 514.5 nm excitation, respectively. The former wavelength was employed for the majority of the experiments; rapid photodecomposition of the thiocyanate complexes occurs when 541.5 nm irradiation was employed.[9] Some adsorbates yielded several Raman bands with sufficient intensity in both the surface and bulk-phase spectra; of particular interest are the C-N stretch (ν_{CN}), N-C-S band (δ_{NCS}), and metal-ammine stretch (ν_{M-NH_3}) for $Cr(NH_3)_5NCS^{2+}$ [9] in comparison with corresponding vibrational modes for NCS^- and hexaammines (Table I).

Several adsorbates were stable over a sufficient potential range to enable the potential dependence of the SEF to be examined. Whereas SEF for thiocyanate decreases marginally with increasing negative potential,[7a] those for pyridine and pyrazine are increased significantly under these conditions (Table I). Of particular interest in this regard is pyrazine-pentaammineosmium; alteration of the potential to values negative of about -350 mV yields reduction of adsorbed Os(III) to Os(II), with consequent large increases in the SER spectral intensities.[8b,c] These changes are associated in part with the occurrence of electronic resonance

for $Os^{II}(NH_3)_5pz$.[8b] We therefore examined this system in greater detail by means of excitation profile measurements in order to ascertain the role of such electronic resonance enhancement in SERS.

Figure 1A shows the electronic absorption spectrum of $Os^{III}(NH_3)_5pz$ in neutral aqueous solution from 300 to 700 nm;[17] this is compared with plots of relative Raman intensities against the excitation wavelength for solution and adsorbed $Os^{III}(NH_3)_5pz$ in Figures 1B and 1C, respectively. The triangles are the integrated intensities of the ν_{12} pyrazine ring mode at 1095 cm^{-1}, whereas the circles refer to the ν_{9a} mode at 1232 cm^{-1}.[8] The intensities of these bands are normalized to each other; the solid line is the "best fit" curve.[18] (Other ring vibrations, such as the ν_1 mode, yielded similar but less pronounced profiles.) While the solution Raman intensities increase rapidly for excitation wavelengths below 500 nm, as expected from the onset of electronic resonance, the SERS intensities increase monotonically with increasing wavelengths from 460 to 676 nm. Figure 2 contains the corresponding information for $Os^{II}(NH_3)_5pz$. The broad electronic absorption peak at 460 nm (Fig. 2A) is associated with a metal-ligand $\pi \rightarrow \pi*$ transition.[17] Peaks are also seen in both the bulk and surface Raman excitation profiles (Fig. 2B and 2C, respectively),[18] although they are shifted to noticeably longer wavelengths, especially for the latter. (The triangles and circles are again intensity normalized to each other and refer here to the ν_{12} mode at 1067 cm^{-1} and the Os-pz stretching mode at 300 cm^{-1},[8] respectively; similar results were also obtained for other pyrazine ring modes.) Figure 3 compares the SERS excitation profile for adsorbed $Os^{II}(NH_3)_5pz$ (solid curve) with that for $Os^{III}(NH_3)_5pz$ (dashed curve) and pyrazine (dashed-dotted curve) plotted on a common intensity scale. It is seen that the pronounced sharp peak at 590 nm for $Os^{II}(NH_3)_5pz$ is essentially absent for the latter two adsorbates.

Discussion

Inspection of the Raman cross sections and surface enhancement factors in Table I reveals several interesting features. Of particular significance is the comparison between SEF values for adsorbates containing common vibrational modes. Similar enhancement factors (within 3 fold) are obtained for ν_{CN} in NCS$^-$ as for the three isothiocyanate complexes, even though the electronic structures of these adsorbates differ substantially. Perhaps more surprisingly, SEF for the ν_{M-NH_3} mode in $Cr(NH_3)_5NCS^{2+}$ is only marginally (2-fold) smaller than for ν_{CN} or δ_{NCS} even though the nonbridging ammine ligands are presumably more distant from, and weakly interacting with, the metal surface. Indeed, the ν_{CN} band for adsorbed $Cr(NH_3)_5NCS^{2+}$ is shifted 30-60 cm^{-1} to higher frequencies and broadened with respect to the bulk phase as a result of adsorbate-surface interactions, whereas the corresponding ν_{M-NH_3} band is scarcely affected.[9]

Nevertheless, SEF of the ν_{M-NH_3} mode for unbound $Cr(NH_3)_6^{3+}$ is significantly (ca. 4 fold) less than that for surface-attached $Cr(NH_3)_5NCS^{2+}$. This latter result may arise from the separation of the hexammine complex from the metal surface by the adsorbed chloride monolayer.[10a] It is instructive to compare also the corresponding bulk-phase and surface Raman cross sections. The bulk Raman cross section for the ν_{M-NH_3} mode of $Cr(NH_3)_6^{3+}$ is substantially (250 fold) higher than that for $Cr(NH_3)_5NCS^{2+}$ (Table I) as a result of the totally symmetric nature of the former. The corresponding 50-fold increase in the SERS cross section for $Cr(NH_3)_6^{3+}$ with respect to $Cr(NH_3)_5NCS^{2+}$ (Table I) indicates a substantial, although smaller, effect of mode symmetry in the surface environment. The smaller SEF for ν_{M-NH_3} in $Cr(NH_3)_6^{3+}$ compared with $Cr(NH_3)_5NCS^{2+}$ can therefore be ascribed to the effective symmetry lowering for the former upon adsorption.

These differences notwithstanding, the variations in the Raman cross sections for the adsorbates in Table I display close similarities in the bulk-phase and surface environments. Equivalently stated, the variations in the surface enhancement factors between the different vibrational modes and adsorbates are substantially less than those of the Raman cross sections themselves. Considering the inevitable uncertainties in the determination of the surface Raman cross sections, these results demonstrate a remarkable insensitivity of the surface enhancement factor to the adsorbate structure and the nature of the adsorbate-surface interactions. It should be noted that the surface Raman cross sections, and hence the surface enhancement factors, assume that every adsorbate molecule contributes equally to the Raman scattering. If, as appears likely,[1b,d,2b] the SERS effect arises from particular morphologies (such as metal clusters) that form only a minority of the total surface sites, the $(d\sigma/d\Omega)_{SER}$ and SEF estimates given here will all be smaller than the actual values by the ratio of the overall to Raman-active site populations.

Turning now to the nitrogen heterocycle-containing systems, both pyridine and pyrazine display SEF values that depend markedly on both the excitation wavelength λ, and the electrode potential. The former dependence is well known since normal Raman scattering intensities are proportional to λ^{-4}, whereas SERS intensities typically increase with increasing λ[1,2]. The latter dependence may be associated with potential-induced changes in the adsorbate orientation. Thus both pyridine and pyrazine may interact with the surface via the nitrogen lone pair and/or the aromatic ring, as well as interact specifically with the adsorbed halide that is necessary for intense SERS with these systems.[19] Pyridine was examined here in part to provide a check on the present SEF measurements by comparison with the

careful determination of SEF for this system by Allen and Van Duyne.[3] Their value for the ν_1 mode at -600 mV using 514.5 nm excitation, 1.3×10^6, is in reasonable agreement with the corresponding value, 8×10^5, in Table I.

The marked differences in the Raman cross sections and surface enhancement factors between pyrazine, $Os^{III}(NH_3)_5pz$ and $Os^{II}(NH_3)_5pz$ (Table I) can be rationalized with the aid of the excitation profiles summarized in Figs. 1 and 2. The ν_1 ring mode has a markedly larger Raman cross section in both Os(III) and Os(II) pyrazine complexes than pyrazine at 647.1 and 514.5 nm, presumably due to preresonance enhancement.[20] For $Os^{III}(NH_3)pz$, this enhancement for ν_1 and other modes is similarly larger in both bulk-phase and surface environments so that the SEF values are relatively unaffected. For $Os^{II}(NH_3)_5pz$, on the other hand, the Raman cross sections for ν_1 and especially ν_{12}, as well as for the osmium-pyrazine stretching mode, ν_{M-pz}, are abnormally large at the surface for 647.1 nm excitation, resulting in extremely high SEF values, approaching 10^8 (Table I). Inspection of Fig. 3 identifies these differences with the onset of resonance enhancement for adsorbed $Os^{II}(NH_3)_5pz$ at 647.1 nm, this effect being essentially absent for adsorbed $Os^{III}(NH_3)_5pz$ and pyrazine. Indeed, Fig. 3 shows that the use of laser wavelengths close to the surface excitation profile peak at 590 nm will yield even larger surface enhancement factors as well as Raman cross sections, since the maximum bulk-phase Raman intensity occurs at a noticeably smaller wavelength.

Often, but by no means always, one finds that the excitation profile peak coincides with the wavelength of maximum absorption.[21] The significantly (ca. 60 nm) higher peak wavelength in the bulk excitation profile (Fig. 2B) than in the absorption spectrum for $Os^{II}(NH_3)_5pz$ may be due in part to

measurement errors, especially in the region below 514 nm where absorption of the incident laser beam may distort the profile. Preresonance effects[20,21] may also contribute, along with resonance coupling to unresolved transitions on the low frequency side of the absorption spectrum. Nevertheless, the SERS excitation profile for $Os^{II}(NH_3)_5pz$ (Fig. 2C) is shifted completely to longer wavelengths. Similar shifts have been reported previously for other adsorbates displaying electronic resonance at silver surfaces[22] and colloids[23]. The underlying reason for these observations is unclear. One possibility is that they are due to a shift in the electronic absorption spectrum or the creation of new electronic states upon adsorption. Thus the $\pi \rightarrow \pi^*$ metal-ligand charge-transfer transition that is responsible for the 460 nm band for $Os^{II}(NH_3)_5pz$ (Fig. 2A)[17a] may shift to longer wavelengths as a result of lower lying π^* states formed by pyrazine-surface interactions. However, these interactions are liable to be weak; indeed the primary impetus for adsorption appears to be electrostatic attraction of the cationic osmium center to coadsorbed chloride.[8b]

A number of other SERS adsorbates that lack electronic resonance effects in bulk media nevertheless yield excitation profile peaks in the 550-700 nm region.[22a,24] Such results can be accounted for by resonant electromagnetic effects associated with localized surface plasmons, or by coupling with adsorbate-surface charge-transfer transitions.[24] However, such "nonspecific" resonance effects appear not to be responsible for the excitation profile peak for adsorbed $Os^{II}(NH_3)_5pz$ since such peaks are essentially absent for adsorbed $Os^{III}(NH_3)_5pz$ and pyrazine (Fig. 3). This result clearly implicates the role of electronic transitions involving the electron added in forming Os(II) from Os(III).

Concluding Remarks

The present results demonstrate that, at least for adsorbates that do not display electronic resonance enhancement in the bulk phase for energies in the vicinity of the Raman excitation, the surface enhancement factors at silver are insensitive to the adsorbate electronic structure and the adsorbate-surface interactions. In particular, SEF values for unattached ("outer-sphere") interfacial species are comparable to those for structurally similar surface-attached ("inner-sphere") adsorbates, even when large variations are seen in the Raman scattering cross sections. For systems having available excited electronic states, however, markedly different surface enhancement factors can be obtained, depending on the irradiation wavelength, due to modification in the Raman excitation profile brought about by adsorption. Nonetheless, the extent of surface Raman enhancement by such electronic effects appears to be roughly comparable to that observed in bulk solution. We have recently initiated systematic SERS studies for a wide variety of adsorbates, including those described here, at gold electrodes.[25,26] The results so far indicate that the enhancement factors are similarly insensitive to the adsorbate structure, although the SERS intensities appear to be more dependent upon the proximity of the vibrational mode to the surface than seen here for silver.

While the present findings do not necessarily preclude the operation of most enhancement mechanisms of the many that have been offered,[1,2] they do provide a quantitative indication that surface attachment ("chemisorption") of the Raman scatterer to the metal surface may in itself exert little influence upon the enhancement factor. In some respects, these results are at odds with the currently popular notion that electrochemical SERS arises from charge-transfer resonance enhancement involving so-called "surface complexes".[27] While the distinction between "surface complex" function and

adsorption is not entirely clear, the attractiveness of such notions is that they can rationalize the sensitivity of SERS to the electrode history as well as to the chemical environment.[28] While the concept of "SERS-active" sites and their necessary stabilization by adsorbate seems reasonable, it would appear that such adsorbate need not be the same species as that responsible for the observed surface Raman signal.[10a] Clearly, most adsorbates that accumulate at metal-electrolyte interfaces in sufficient concentrations to yield observable SERS will also bind directly to the Raman-active sites; this does not, however, imply that the former finding is a consequence of the latter. Thus for SERS of $Cr(NH_3)_6^{3+}$, for example, such site stabilization is provided by nearby specifically adsorbed halide, whereas $Cr(NH_3)_5NCS^{2+}$ is able to bind directly via the thiocyanate linkage.[10a]

The extent that "surface resonance" enhancement models involving adsorbate-surface charge transfer require surface attachment of the adsorbate to be valid is unclear at present. As we have noted previously,[10a] efficient electron tunneling can occur even for unbound molecules close to (within 4-6 Å of) the metal surface.[29] In any case, the present findings do illustrate that SERS models that require molecules to be bound chemically to form some "surface complex" are in some respects unnecessary.[27] Perhaps more importantly from our point of view, these results also provide some further reassurance that SERS can be employed to probe the structural and dynamical properties of adsorbates at metal surfaces without an accompanying obligation to unravel the last details of the underlying enhancement mechanisms.

Acknowledgments

References

1. For reviews, (a) Van Duyne, R. P., in "Chemical and Biochemical Applications of Lasers", Vol. 4, Moore, C. B.; ed, Academic Press, N.Y., 1979, Chapter 5; (b) Chang, R. K.; Furtak, T. E.; "Surface-Enhanced Raman Scattering"; Plenum Press, N.Y.; 1982; (c) Burke, R. L.; Lombardi, J. R.; Sanchez, L. A.; Adv. Chem. Ser., 1982, 201, 69; (d) Chang, R. K.; Laube, B. L.; CRC Crit. Rev. Solid State Mat. Sci., 1984, 12, 1.

2. For reviews, (a) Furtak, T. E.; Reyes, J.; Surface Sci. 1980, 93, 382; (b) Otto, A., in "Light Scattering in Solids", Cardona, M.; Guntherodt, G., eds., Springer, Berlin, 1984.

3. Allen, C. S.; Van Duyne, R. P., unpublished observations quoted in ref. (1a).

4. Busby, C. C., Creighton, J. A.; J. Electroanal. Chem. 1982, 133, 183.

5. (a) Guyer, K. L.; Weaver, M. J.; Inorg. Chem., 1984, 23, 1664; (b) Guyer, K. L.; Barr, S. W.; Weaver, M. J.; in "Proc. Symp. on Electrocatalysis", W. E. O'Grady, P. N. Ross, Jr., F. G. Will, eds, Electrochemical Society, Pennington, N.J.; 1982, p. 377.

6. (a) Hupp, J. T.; Larkin, D.; Weaver, M. J.; Surf. Sci. 1983, 125, 429; (b) Larkin, D.; Guyer, K. L.; Hupp, J. T.; Weaver, M. J.; J. Electroanal. Chem. 1982, 138, 401.

7. (a) Weaver, M. J.; Barz, F.; Gordon II, J. G.; Philpott, M. R.; Surf. Sci. 1983, 125, 409; (b) Weaver, M. J.; Hupp, J. T.; Barz, F.; Gordon II, J. G.; Philpott, M. R.; J. Electroanal. Chem., 1984, 160, 321.

8. (a) Farquharson, S.; Weaver, M. J.; Lay, P. A.; Magnuson, R. H.; Taube, H.; J. Am. Chem. Soc. 1983, 105, 3350; (b) Farquharson, S.; Guyer, K. L.; Lay, P. A.; Magnuson, R. H.; Weaver, M. J.; J. Am. Chem. Soc., 1984, 106, 5123; (c) Farquharson, S.; Lay, P. A.; Weaver, M. J.; Spectrochim. Acta 1984, 40A, 907.

9. Tadayyoni, M. A.; Farquharson, S.; Li, T. T-T.; Weaver, M. J.; J. Phys. Chem., 1984, 88, 4701.

10. (a) Tadayyoni, M. A.; Farquharson, S.; Weaver, M. J.; J. Chem. Phys., 1984, 80, 1363; (b) Farquharson, S.; Milner, D.; Tadayyoni, M. A.; Weaver, M. J.; J. Electroanal. Chem. 1984, 178, 143.

11. Bauer, G. (Ed); "Handbook of Preparative Inorganic Chemistry", Vol. 2, 2nd Ed, Academic Press, N.Y.; 1965, p. 1351, 1531.

12. (a) Skinner, J. G.; Nilsen, W. G.; J. Opt. Soc. Am. 1968, 58, 113; (b) Kato, Y.; Takuma, H.; J. Opt. Soc. Am. 1971, 61, 347.

13. Gennett, T.; Hupp, J. T.; Weaver, M. J.; to be published.

14. Tadayyoni, M. A.; Weaver, M. J.; J. Electroanal. Chem., in press.

15. Li, T. T-T.; Weaver, M. J.; J. Am. Chem. Soc. 1984, 106, 1233.

16. The surface concentrations listed in Table I are computed on the basis of the apparent (i.e., geometrical), rather than the real (i.e., microscopic) surface area. The roughness factor (i.e., the ratio of microscopic to geometrical surface areas) for the roughened silver electrodes was typically in the range ca. 1.5 to 2.5.[6a]

17. (a) Magnuson, R. H.; Taube, H.; J. Am. Chem. Soc. 1975, 97, 5129; (b) Sen, J.; Taube, H.; Acta. Chem. Scand. 1979, A33, 125.

18. The bulk Raman intensities in Figs. 2B and 3B were normalized as a function of excitation wavelength, λ, for both the spectrometer throughput and the dependence upon λ^{-4} anticipated for normal Raman scattering by correction for the wavelength-dependent intensities observed under the same conditions for the 992 cm^{-1} band of liquid benzene. The surface Raman intensities in Figs. 2C and 3C, however, were corrected in this manner only for the wavelength-dependent throughput of the spectrometer.

19. See for example, Fleischmann, M.; Hill, I. R.; J. Electroanal. Chem., 1983, 146, 353.

20. For a review, see Clark, R. J. H., in "Advances in Infrared and Raman Spectroscopy", R. J. H. Clark, R. E. Hester, eds., Vol. 1, Heyden (pub), London, 1975, Chapter 4.

21. For reviews, see (a) Johnson, B. B.; Peticolas, W. L.; Ann. Rev. Phys. Chem. 1976, 27, 465; (b) Spiro, T. G.; Stein, P.; ibid, 1977, 28, 501.

22. (a) Blatchford, C. G.; Campbell, J. R.; Creighton, J. A.; Surf. Sci. 1981, 108, 411; (b) Chambers, J. A.; Buck, R. P.; J. Electroanal. Chem. 1984, 163, 297.

23. (a) Siiman, O.; Bumm, L. A.; Callaghan, R.; Blatchford, C. G.; Kerker, M.; J. Phys. Chem. 1983, 87, 1014; (b) Siiman, O.; Lepp, A.; Kerker, M.; J. Phys. Chem. 1983, 87, 5319.

24. For a short review, see Seki, H.; J. Electron Spect. Related Phen. 1983, 29, 413; see also Seki, H.; J. Electroanal. Chem. 1983, 150, 425; Pockrand, I.; Billman, J.; Otto, A.; J. Chem. Phys. 1983, 78, 6384.

25. Gao, P.; Patterson, M. L.; Tadayyoni, M. A.; Weaver, M. J.; Langmuir, in press.

26. Gao, P.; Weaver, M. J.; unpublished results.

27. There has been surprisingly vigorous support for the general applicability of such a "surface complex" model of SERS, see, for example, Roy, D.; Furtak, T. E.; J. Chem. Phys. 1984, 81, 4168.

28. For example, Wanatabe, T.; Kawanami, O.; Honda, K.; Pettinger, B.;
    Chem. Phys. Lett. 1983, 102, 565.

29. Hupp, J. T.; Weaver, M. J.; J. Phys. Chem. 1984, 88, 1860.

TABLE I Raman Scattering Cross Sections (cm² steradians⁻¹ molecule⁻¹) of Representative Adsorbates in Bulk Solution and at Silver Electrodes, and Surface Enhancement Factors.

Adsorbate[a]	C_b[b] mM	$\Gamma \times 10^{11}$ [o] mole cm⁻²	Mode[d]	$n^{-1}\left(\frac{d\sigma}{d\Omega}\right)_{BR} \times 10^{29}$ [e]	$n^{-1}\left(\frac{d\sigma}{d\Omega}\right)_{SER} \times 10^{23}$ [f]	SEF $\times 10^{-6}$
NCS^-	≥ 1.0[h,i]	400[n,v,x]	ν_{CN}	0.4[p,q,u]	0.5^v , 0.3^x	1.2^v
$Cr^{III}(NCS)_6^{3-}$	1.0[i,j]	50[o,v]	ν_{CN}	0.25[p,u]	0.25^v	1.0^v
$Cr^{III}(NH_3)_5NCS^{2+}$	1.0[i,j,k]	60[o,v]	ν_{CN}	0.075^u	0.23^v	3.0^v
			ν_{M-NH_3}	0.020^u	0.03^v	1.5^v
			δ_{NCS}	0.080^u	0.25^v	3.0^v
$t\text{-}Cr^{III}(NH_3)_2(NCS)_4^-$	1.0^j	40[o,v]	ν_{CN}	0.28^q	0.85^v	3.0^v
$Cr^{III}(NH_3)_6^{3+}$	0.05^j	~ 5[o,v]	ν_{M-NH_3}	5.1[p,u]	1.7^v	0.35^v
$Co^{III}(NH_3)_6^{3+}$	0.05^l	5[o,w]	ν_{M-NH_3}	1.0[p,q]	0.4^w	0.4^w
pyridine	10^h	~ 100[n,x], ~ 50[n,x]	ν_1	0.42^p	$\sim 0.2^w$, $\sim 3^x$	0.5^w, $\sim 7^x$
				$(1.1)^p$	$(0.1)^w$, $(0.8)^x$	$(0.1)^w$, $(0.8)^x$
pyrazine	10^h	~ 50[n,x], ~ 20[n,x]	ν_1	1.6^p	$\sim 1.5^w$, $\sim 10^x$	$\sim 1.0^w$, 6^x
$Os^{III}(NH_3)_5py^{3+}$	0.1^m	15°	ν_1	57^p	5.5^y	0.1^y
$Os^{III}(NH_3)_5pz^{3+}$	0.1^h	$\sim 10^o$	ν_1	24^p	28^y	1.1^y
			ν_{12}	$(26)^p$	$(11)^y$	$(0.4)^y$
				9.9^p	10^y	1.0^y
			ν_{9a}	$(10.5)^p$	$(8)^y$	$(0.75)^y$
				$(8.5)^p$	$(7)^y$	$(0.8)^y$
$Os^{II}(NH_3)_5pz^{2+}$	0.1^h	$\sim 10^o$	ν_1	12.8^p	50^z	4.0^z
				$(8)^p$	$(35)^z$	$(4.5)^z$
			ν_{12}	12.8^p	300^z	23^z
				$(190)^p$	$(225)^z$	$(1.2)^z$

	ν_{M-pz}		
	6.5^p	550^z	85^z
	$(12.8)^p$	$(250)^z$	$(20)^z$

Table I Continued

_____

Footnotes to Table I

[a] py = pyridine ligand; pz = pyrazine ligand

[b] Bulk adsorbate concentration (mM) corresponding to surface concentration, Γ, at which SER spectra were obtained. Supporting electrolyte was 0.1 $\underline{M}$ KCl, except where indicated.

[c] Surface concentration of adsorbate (mole cm^{-2}),[16] determined by using technique indicated.

[d] Vibrational mode: ν_{CN} = C–N stretch;[7a,9] ν_{M-NH_3} = metal–ammine stretch;[9,10] δ = N–C–S bend;[7a,9] ν_{M-pz} = metal–pyrazine stretch;[8] ν_1, ν_{6b}, ν_{8a}, ν_{9a} = pyridine or pyrazine ring modes, identified with Wilson mode number as subscript.

[e] Raman scattering cross section of given vibrational mode for bulk solution species ($\times 10^{29}$ cm^2 steradian^{-1} molecule^{-1}) divided by number of functional groups per molecule, n. Determined by calibration with liquid benzene, as outlined in text. Solution conditions as indicated. Values in parentheses determined for 514.5 nm excitation wavelength; otherwise at 647.1 nm.

[f] Raman scattering cross section ($\times 10^{23}$ cm^2 steradian^{-1} molecule^{-1}) of given vibrational mode for adsorbed species at silver–aqueous interface, divided by number of functional groups per molecule, n. Measured at electrode potential as indicated. Determined from integrated intensity of SER spectra along with listed values of Γ as outlined in text. Values in parentheses at 514.5 nm; otherwise 647.1 nm.

[g] Surface enhancement factor ($\times 10^{-6}$) at electrode potential as indicated, from ratio of surface. to bulk-phase Raman scattering cross sections [Eq. (1)]. Values in parentheses at 514.5 nm; otherwise at 647.1 nm laser excitation.

Footnotes to Table I Continued

h 0.1 M KCl

i 0.1 M NaClO$_4$ + 2 mM HClO$_4$

j 0.1 M KCl + 2 mM HCl

k 0.01 M KCl + 2 mM HCl

l 0.1 M NaClO$_4$ + 10 mM NaCl + 2 mM HCl

m 0.1 M HCl

n Determined from differential capacitance-potential curves. For NCS$^-$, see refs. 6a, 7a; for pyridine, pyrazine, see text and ref. 13.

o Determined from rapid linear sweep voltammetry. For NCS$^-$ complexes see ref. 14; for Cr(NH$_3$)$_6$$^{3+}$, Co(NH$_3$)$_6$$^{3+}$ see refs. 10, 15 and the text; for osmium complexes, see ref. 8b.

p Determined in aqueous solution (generally 0.01-1 M, depending on magnitude of scattering cross section).

q Determined in dimethylsulfoxide solution (generally 0.1-1 M).

u Determined in Nujol mull (ca. 1 M).

v -300 mV. vs s.c.e.

w -100 mV. vs s.c.e.

x -600 mV. vs s.c.e.

y -150 mV. vs s.c.e.

z -550 mV. vs s.c.e.

Figure Captions

Figure 1

Comparison of solution absorption spectrum with bulk-phase and surface Raman excitation profiles for $Os^{III}(NH_3)_5pz$ (pz = pyrazine).

A) Absorption spectrum for ca. 2 m$\underline{M}$ $Os^{III}(NH_3)_5pz$ in 0.1 $\underline{M}$ NaCl, pH 9. The peak at 325 nm has a molar absorptivity of 1.5×10^3.[17b]

B) Raman excitation profiles for above solution from 460 to 647 nm. Circles and triangles are integrated intensities of ν_{9a} (1235 cm^{-1}) and ν_{12} (1095 cm^{-1}) modes, respectively, of coordinated pyrazine, normalized to each other at maximum intensity (see footnote 18). Solid curve is estimated best fit through experimental points.

C) As for B, but for SERS intensities at silver electrode at -150 mV vs s.c.e.

Figure 2

Comparison of solution absorption spectrum with bulk-phase and surface Raman excitation profiles for $Os^{II}(NH_3)_5pz$.

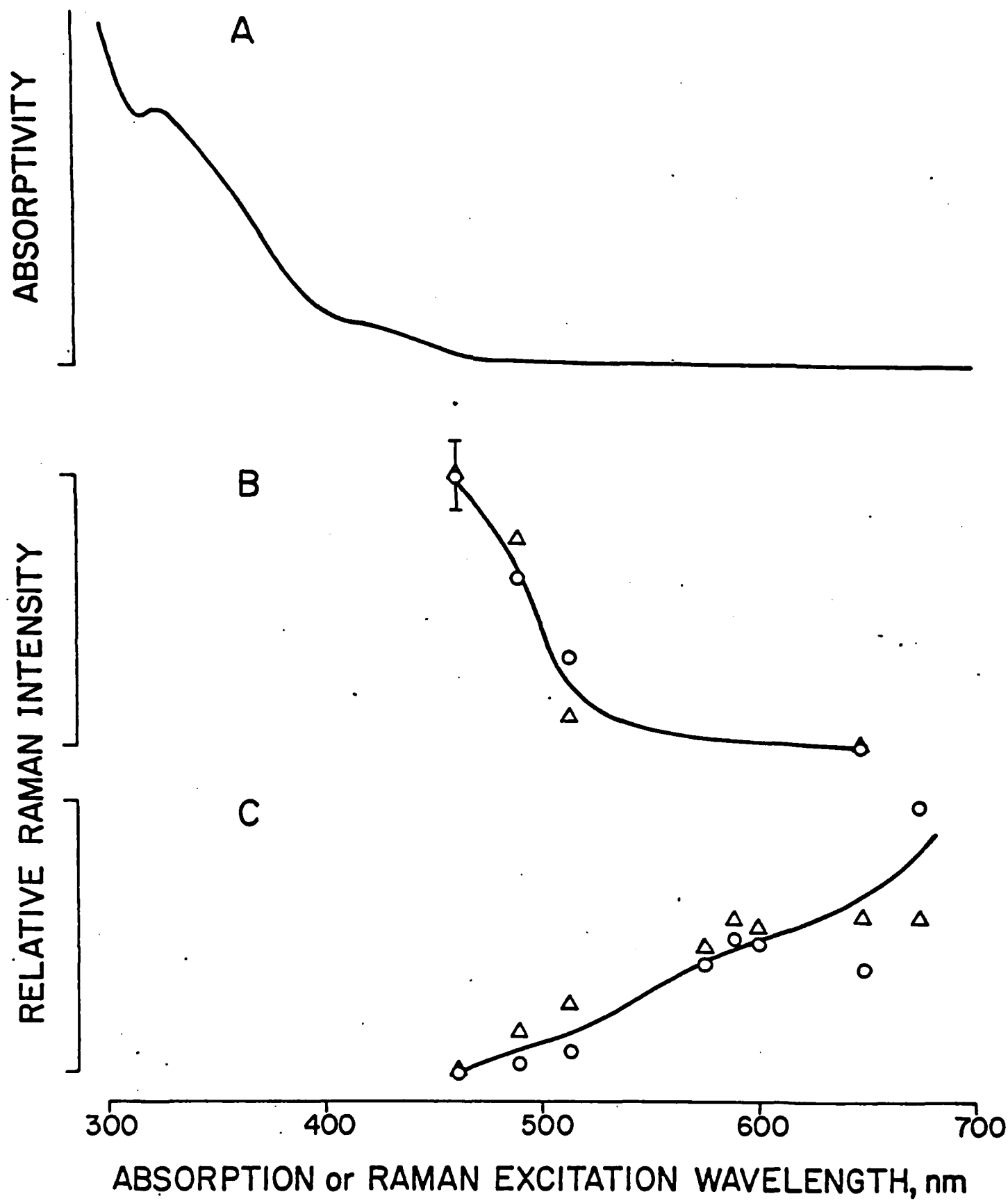A) Absorption spectrum for ca. 2 m$\underline{M}$ $Os^{II}(NH_3)_5pz$ in 0.1 $\underline{M}$ NaCl, pH 9. The peak at 460 nm has a molar absorptivity of 7×10^3.[17b]
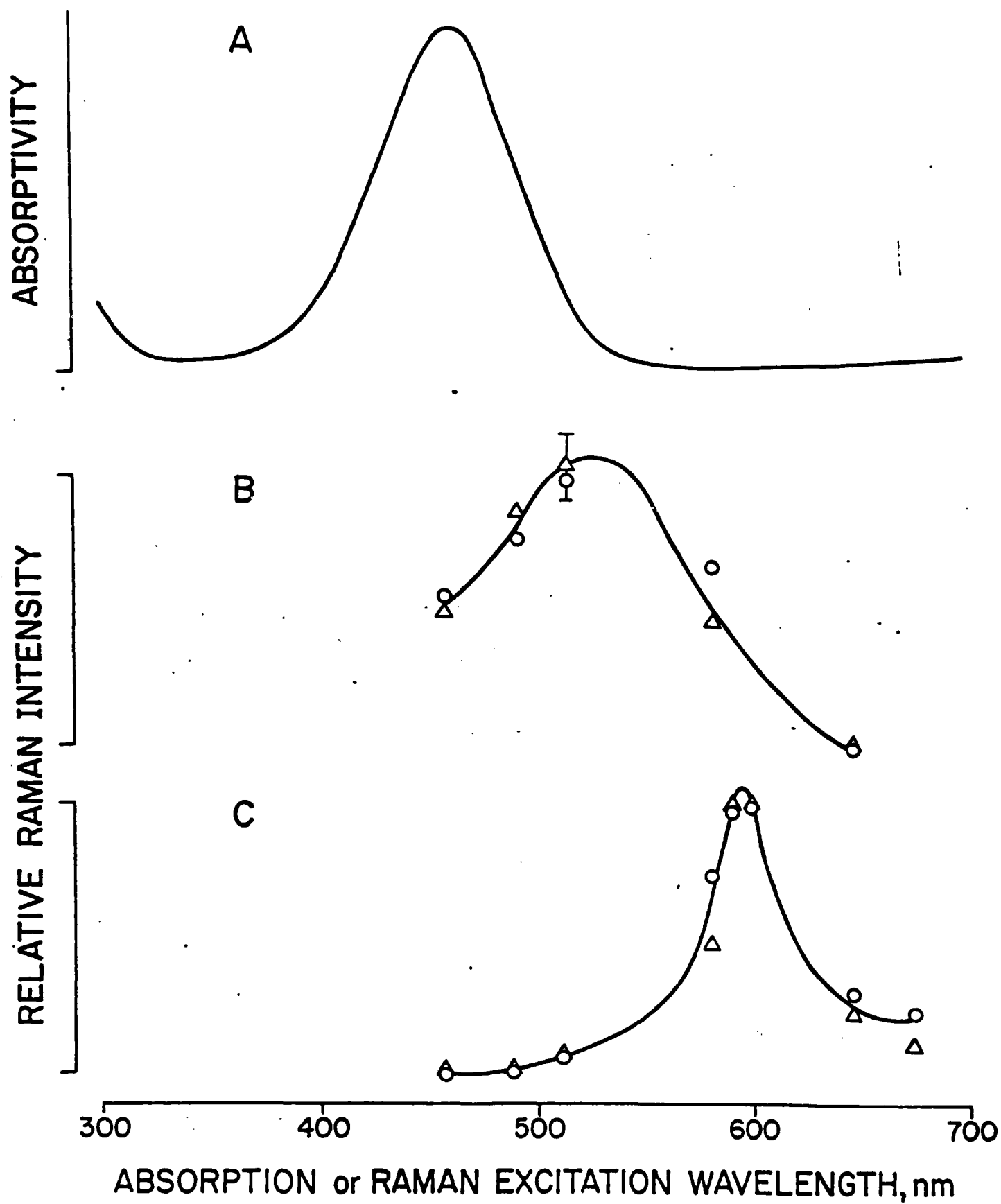
B) Raman excitation profiles for above solution from 460 to 647 nm. Circles and triangles are integrated intensities of metal-pyrazine stretching (ca. 300 cm^{-1}) and ν_{12} pyrazine ring (1070 cm^{-1}) modes, respectively, normalized to each other at maximum intensity (see footnote 18). Solid curve is estimated best fit through experimental points.

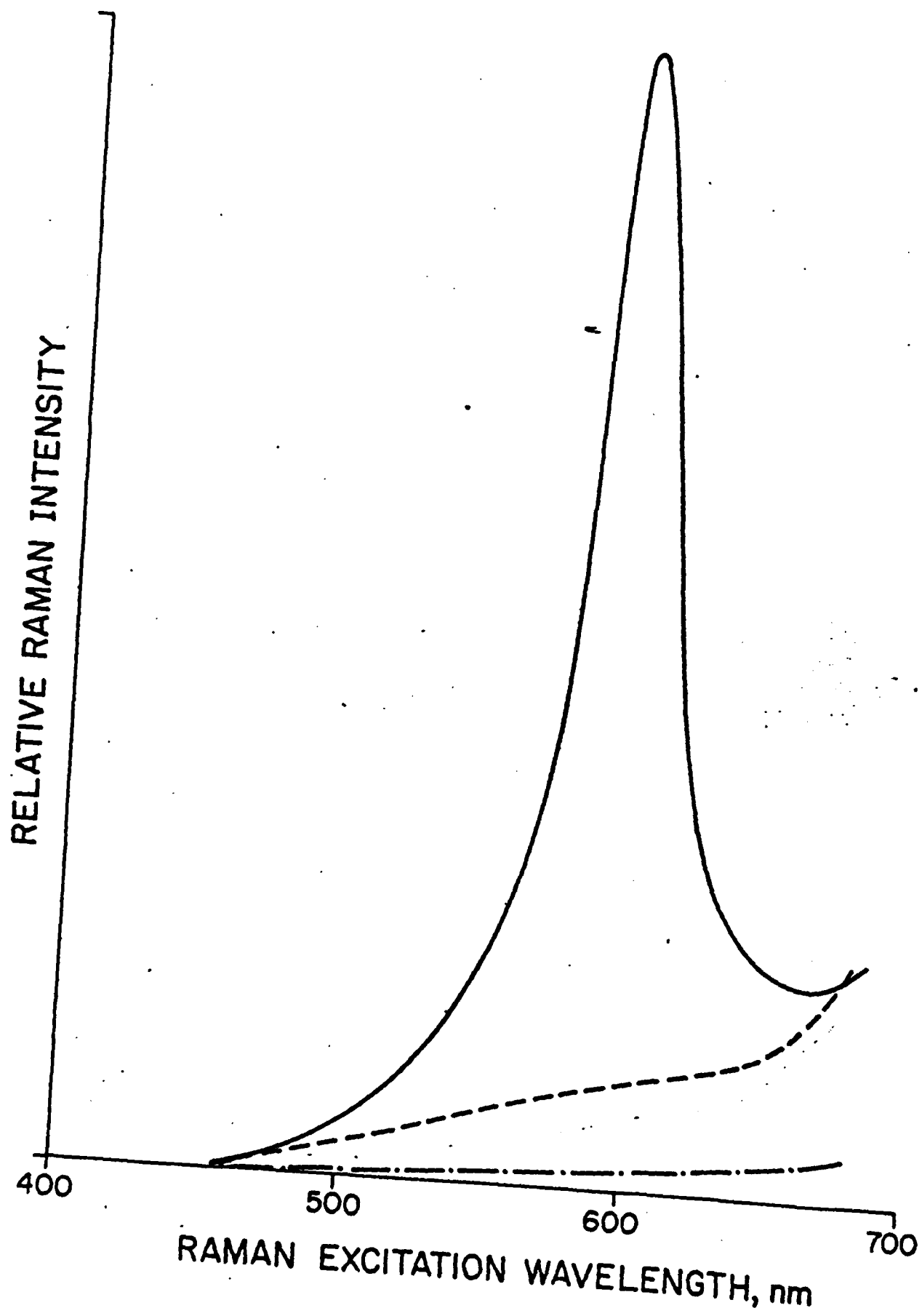C) As for B, but for SERS intensities at silver electrode at -550 mV vs s.c.e.

Figure 3

Comparison between SERS excitation profiles at silver electrodes for ν_{12} pyrazine ring mode in adsorbed $Os^{II}(NH_3)_5pz$ (solid curve), $Os^{III}(NH_3)_5py$ (dashed curve), and pyrazine (dashed-dotted curve), plotted on common Raman intensity scale. Conditions as in Table I; plots are estimated best-fit curves from Figures 1 and 2.

ABSORPTION or RAMAN EXCITATION WAVELENGTH, nm

ABSORPTION or RAMAN EXCITATION WAVELENGTH, nm

RELATIVE RAMAN INTENSITY

RAMAN EXCITATION WAVELENGTH, nm

400 500 600 700

3

END

FILMED

11-85

DTIC